Linear regression analysis of buffeting response under skew wind

Zengwei Guo, Yaojun Ge[*], Lin Zhao and Yahui Shao

State Key Laboratory of Disaster Reduction in Civil Engineering, Department of Bridge Engineering, Tongji University, shanghai 200092, P. R. China

Abstract. This paper presents a new analysis framework for predicting the internal buffeting forces in bridge components under skew wind. A linear regressive model between the internal buffeting force and deformation under normal wind is derived based on mathematical statistical theory. Applying this regression model under normal wind and the time history of buffeting displacement under skew wind with different yaw angles in wind tunnel tests, internal buffeting forces in bridge components can be obtained directly, without using the complex theory of buffeting analysis under skew wind. A self-anchored suspension bridge with a main span of 260 m and a steel arch bridge with a main span of 450 m are selected as case studies to illustrate the application of this linear regressive framework. The results show that the regressive model between internal buffeting force and displacement may be of high significance and can also be applied in the skew wind case with proper regressands, and the most unfavorable internal buffeting forces often occur under yaw wind.

Keywords: bridge; linear regression; skew wind; buffeting; internal force

1. Introduction

Buffeting is a phenomenon of stochastic forced vibration caused by turbulence existing inherently in natural wind in conjunction with structural-induced signature turbulence. With increasing lengths of main spans, buffeting responses may rapidly increase, resulting in substantial increases in stresses and serious fatigue damage to bridge components and connections. Therefore, it is becoming increasingly important to predict wind-induced internal buffeting forces in components of long-span bridges.

Wind tunnel tests on full bridge aero-elastic models will continue to be indispensable for evaluating wind induced vibrations of long-span bridges (Zhu *et al.* 2007). As full bridge aero-elastic models usually use core beams to simulate the stiffness systems of real bridges, the similarity relations of displacement may be explicit, but there are no similarity relations for internal forces in bridge components. Therefore, internal buffeting forces in real bridges cannot be obtained from wind tunnel tests directly according to similarity law. Fortunately, numerical analysis based on the finite element method and the semi-empirical model of wind forces can

∗Corresponding author, Professor, E-mail: yaojunge@tongji.edu.cn

predict these forces. However, most existing buffeting analysis methods are based on the assumption that the incident mean wind is perpendicular to the longitudinal axis of the bridge (Davenport 1962, Lin 1979, Scanlan 1978). This may not always be the case when the bridge is located in a complex heterogeneous topography and is attacked by a typhoon (Zhu and Xu 2005). In order to consider skew wind effects in buffeting analysis, most researches dispose the mean yaw wind into one component normal and one parallel to the longitudinal axis of the bridge (Kimura and Tanaka 1992, Scanlan 1993a, Xie *et al.* 1991). This method of considering mean yaw wind may meet some intractable issues, such as how to decompose velocity fluctuations of turbulent wind, how to determinate the span-wise coherence function of the decomposed turbulent wind and how to compose the calculated response components induced by the two decomposed turbulent wind components. Zhu has presented a finite-element-based framework for buffeting analysis of long-span bridges under skew winds in the frequency domain (Zhu *et al.* 2002, Zhu *et al.* 2002, Zhu and Xu 2005). However, it is necessary to identify aerostatic and aerodynamic parameters, such as mean static coefficients, aerodynamic derivatives and aerodynamic admittance functions. As these aerostatic and aerodynamic parameters are all functions of geometric configuration, wind attack angle and yaw angle of bridge sections, massive sectional model wind tunnel tests need to be carried out for different wind attack angles and yaw angles. In addition, complicated coordinate transformation is necessary.

We applied mathematical statistics to illustrate a framework of a linear regression analysis of internal buffeting forces under skew wind by combining numerical buffeting analysis under normal wind and full bridge aero-elastic model wind tunnel testing under skew wind. To illustrate the effectiveness of this regression method, we applied it to a self-anchored suspension bridge with a main span of 260m and a steel arch bridge with a main span of 450 m as case studies.

2. Framework of linear regression analysis of buffeting internal force

For linearly elastic structures, the relationship between internal force and deformation induced by buffeting vibration can be considered statistically as a linear transformation. The theory of buffeting analysis under normal wind is quite reliable: numerical analysis results fit well with wind tunnel testing results (Zhao *et al.* 2008). As the theory of buffeting numerical analysis under skew wind is relatively complicated and fuzzy, it is not appropriate to predict internal buffeting forces in bridge components under yaw wind. The regression analysis framework for internal buffeting forces under skew wind is implemented as follows:

(1) The stochastic velocity fluctuations of turbulent wind, the finite element model and the aerodynamic parameters used in numerical analysis are first checked by comparing the buffeting displacement obtained in wind tunnel tests with numerical results under normal wind.

(2) The objective internal forces in bridge components are determined firstly, and the displacements used in the regression analysis are selected according to these forces and the dominant modes inducing buffeting response under normal wind.

(3) The regression equations between buffeting displacement and internal force are established based on the time history of numerical results under normal wind.

(4) The significance of the regression equations and regression coefficients are analyzed to ensure they are of high significance.

(5) The similarity of dominant modes participating in buffeting response and the corresponding mode participation coefficients under normal wind and skew wind are investigated to determine

the applicability of the regression equations for normal wind to prediction of internal forces in bridge components under skew wind.

(6) The objective internal buffeting forces under skew wind with different yaw angles are predicted using the buffeting displacements under skew wind obtained from wind tunnel testing and the regression equations.

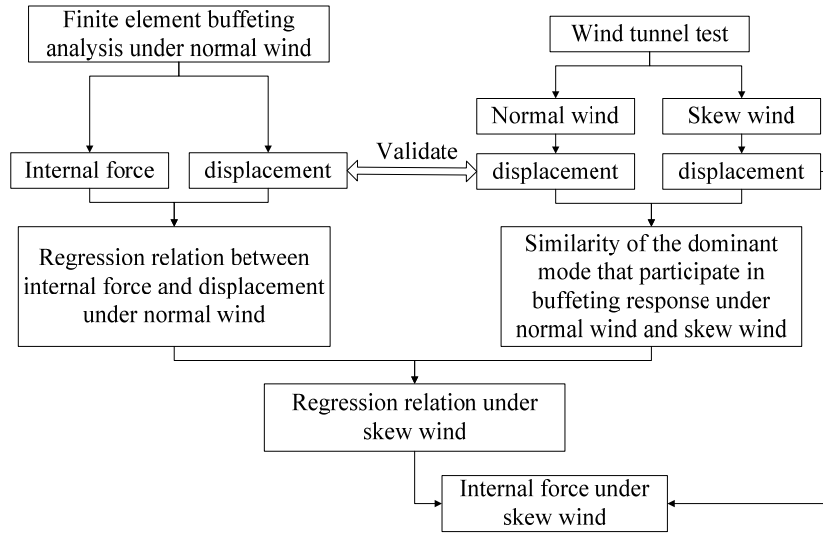This framework is described concisely in Fig. 1.

Fig. 1 Regression analysis framework for determining internal buffeting force under skew wind

3. Formulation of regression analysis of buffeting response

In this analysis, the internal buffeting forces in bridge components are denoted as $\mathbf{F}$. They are also called regressors and are mainly influenced by displacements $\mathbf{\Delta}$. Considering the random variation of $\mathbf{F}$, normal random variables $\mathbf{\varepsilon}$ with zero mean are also added to the equations. Therefore, the linear regression equations between internal buffeting force and displacement of bridge take the following form

$$\begin{cases} \mathbf{F} = \mathbf{\Delta}\mathbf{\beta} + \mathbf{\varepsilon} \\ \mathbf{\varepsilon} \sim N(0, \sigma^2) \end{cases} \tag{1}$$

where $\mathbf{\Delta} = \begin{bmatrix} 1 & \delta_{11} & \cdots & \delta_{1m} \\ \vdots & \vdots & \cdots & \vdots \\ 1 & \delta_{n1} & \cdots & \delta_{nm} \end{bmatrix}, \mathbf{F} = \begin{bmatrix} F_1 \\ \vdots \\ F_n \end{bmatrix}, \quad \mathbf{\varepsilon} = [\varepsilon_1 \quad \cdots \quad \varepsilon_n]^T, \quad \mathbf{\beta} = [\beta_0 \quad \beta_1 \quad \cdots \quad \beta_m]^T, m$

indicates the number of displacements in the regressive model and n indicates the length of sampling.

Using the least-square estimation method, the point estimation of the regression coefficients $\boldsymbol{\beta}$ can be given as

$$\hat{\boldsymbol{\beta}} = (\boldsymbol{\Delta}^T\boldsymbol{\Delta})^{-1}\boldsymbol{\Delta}^T\mathbf{F} \tag{2}$$

The statistical variables, $\tilde{F}$ and R, which can be used to check out the significance of regression equation, are defined as

$$\tilde{F} = \frac{\sum_{i=1}^{n}\left(\hat{F}_i - \bar{F}\right)^2 \Big/ m}{\sum_{i=1}^{n}\left(F_i - \hat{F}_i\right)^2 \Big/ (n-m-1)} \sim F(m, n-m-1) \tag{3}$$

$$R = \sqrt{\sum_{i=1}^{n}\left(\hat{F}_i - \bar{F}\right)^2 \Big/ \sum_{i=1}^{n}\left(F_i - \bar{F}\right)^2} \tag{4}$$

where $F(m, n-m-1)$ indicates the statistical variable $\tilde{F}$ obeys F-distribution, and R indicates the correlation coefficient of linear regression.

If all the absolute values of regression coefficients $\boldsymbol{\beta}$ are close to zero, the regression relation between objective internal force and displacement is not significant. Therefore, the null hypotheses can be expressed as

$$H_0\colon \beta_j = 0 \ (j=1\cdots m) \tag{5}$$

If $F > F_{1-\alpha}(m, n-m-1)$, the null hypotheses can be rejected. Besides, the greater the variable R is, the more significant the regression equation. If $R > 0.8$, the regressive model is linearly correlated to a high confidence level.

The significant regression equation does not represent that all the absolute values of regression coefficients in the regression equations are much greater than zero. If the absolute value of β_j approaches zero, the relation between displacement δ_j and objective internal force $\mathbf{F}$ is not linearly significant. Therefore, the null hypotheses can be expressed as

$$H_0^{(j)}\colon \beta_j = 0 \tag{6}$$

The statistical variables, t_j, which can be used to check out the significance of the regression coefficients, are defined as

$$t_j = \frac{\hat{\beta}_j \Big/ \sqrt{diag\left[\left(\boldsymbol{\Delta}^T\boldsymbol{\Delta}\right)^{-1}\right]_{jj}}}{\sqrt{\sum_{i=1}^{n}(F_i - \hat{F}_i)^2 /(n-m-1)}} \sim t(n-m-1) \tag{7}$$

where $t(n-m-1)$ indicates that the statistical variable t_j obeys the student distribution. If

$|t_j|>t_\alpha(n\text{-}m\text{-}1)$, the null hypotheses can be rejected.

After the significance of the regressive model and regression coefficients have been tested, given the displacement $\mathbf{\Delta}_0$ determined from Eq. (2) and $\boldsymbol{\beta}$ is substituted in Eq. (8), the value of $\hat{\mathbf{F}}$ can be estimated as

$$\hat{\mathbf{F}} = \mathbf{\Delta}\hat{\boldsymbol{\beta}} \tag{8}$$

4. Buffeting analysis in time domain under normal wind

The governing equations of motion of a bridge subjected to winds are given in matrix form as

$$\mathbf{M}\ddot{\mathbf{X}} + \mathbf{C}\dot{\mathbf{X}} + \mathbf{K}\mathbf{X} = \mathbf{F}_G + \mathbf{F}_{st} + \mathbf{F}_b + \mathbf{F}_{se} \tag{9}$$

where $\mathbf{M}$, $\mathbf{C}$, and $\mathbf{K}$=mass, damping, stiffness matrices, respectively; $\mathbf{X}$=nodal displacement vector, and the head dot denotes partial differentiation with respect to time t; $\mathbf{F}$ indicates the nodal force vector, and subscripts G, st, b, and se denote gravity force, time-averaged aerostatic force, time-varying buffeting force and self-excited force, respectively.

Buffeting response can be analyzed in the time or frequency domain. In the present paper, the Newmark-β integration method is utilized. Firstly, the wind forces acting on the bridge components should be simulated and discretized. The time-averaged aerostatic forces acting on per unit length of a bridge's components can be defined by static coefficients, and time-varying buffeting forces and self-excited forces can be simulated using the semi-empirical models suggested by Davenport and Scanlan (Davenport 1962, Scanlan 2000). To convert these uniformly distributed forces into element-end forces, a simple lumping procedure is adopted whereby one half of the element load is acting upon each element node.

Specifically, the aerostatic force components applied to one node of a discrete element with the length of L_e can be expressed in wind axes as

$$L_{st} = \frac{1}{4}\rho U^2 B L_e C_L(\alpha) \tag{10a}$$

$$D_{st} = \frac{1}{4}\rho U^2 B L_e C_D(\alpha) \tag{10b}$$

$$M_{st} = \frac{1}{4}\rho U^2 B^2 L_e C_M(\alpha) \tag{10c}$$

where L_{st}, D_{st}, M_{st}=lift, drag, and pitching moment force component of mean static force, respectively; ρ=air density; U=mean wind velocity; B=bridge deck width; C_L, C_D and C_M=mean lift, drag and pitching moment coefficients, respectively; and α= attack angle of wind.

In addition, the time-varying self-excited force acting per unit length of bridge deck can be expressed as (Scanlan 2000)

$$L = \frac{1}{2}\rho U^2 \left(2B\right)\left(KH_1^* \frac{\dot{h}}{U} + KH_2^* \frac{B\dot{\alpha}}{U} + K^2 H_3^* \alpha + K^2 H_4^* \frac{h}{B} + KH_5^* \frac{\dot{p}}{U} + K^2 H_6^* \frac{p}{B} \right) \quad (11a)$$

$$D = \frac{1}{2}\rho U^2 \left(2B\right)\left(KP_1^* \frac{\dot{p}}{U} + KP_2^* \frac{B\dot{\alpha}}{U} + K^2 P_3^* \alpha + K^2 P_4^* \frac{p}{B} + KP_5^* \frac{\dot{h}}{U} + K^2 P_6^* \frac{h}{B} \right) \quad (11b)$$

$$M = \frac{1}{2}\rho U^2 \left(2B^2\right)\left(KA_1^* \frac{\dot{h}}{U} + KA_2^* \frac{B\dot{\alpha}}{U} + K^2 A_3^* \alpha + K^2 A_4^* \frac{h}{B} + KA_5^* \frac{\dot{p}}{U} + K^2 A_6^* \frac{p}{B} \right) \quad (11c)$$

where $K=\omega B/U$; ω=circular frequency; h, p, α=vertical, lateral and pitching displacement; and H_i^*, A_i^*, P_i^* (i=1,2,···6)=frequency dependent flutter derivative.

As the flutter derivatives are frequency dependent, it is more reasonable to use the unsteady self-excited force model expressed in the time domain, which are conventionally expressed in terms of convolution integrals of the impulse response functions (Lin and Li 1983, Scanlan 1993b) or indicial response functions (Borri *et al.* 2002, Salvatori and Borri 2007), while additional nonlinear convolution integral terms may be introduced in order to consider the unsteady fluid memory effect of self-exited force. In this study, however, the self-exited forces are considered in Scanlan's form, and the flutter derivatives are determined accordding to the fundamental vertical, lateral and pitching frequencies of bridge and the design reference wind speed at the bridge deck level.

The effects of self-exited force can be considered in the manner of aerodynamic stiffness and aerodynamic damping. In finite element analysis, additional aerodynamic elements (Ge and Tanaka 2000), as shown in Fig. 2, are appended in the structural elements to consider the effects of self-exited force.
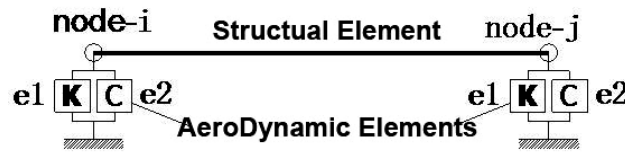

Fig. 2 the aerodynamic element of self-excited force

The matrix of aerodynamic stiffness element and aerodynamic damping element are given as

$$\mathbf{K}_{ae}^e = \begin{bmatrix} \mathbf{K}_{ae1}^e & \mathbf{0} \\ \mathbf{0} & \mathbf{K}_{ae1}^e \end{bmatrix}, \quad \mathbf{C}_{ae}^e = \begin{bmatrix} \mathbf{C}_{ae1}^e & \mathbf{0} \\ \mathbf{0} & \mathbf{C}_{ae1}^e \end{bmatrix} \quad (12,a,b)$$

where

$$\mathbf{K}_{ae1}^{e} = -\frac{1}{2}\rho U^2 L_e K^2 \begin{bmatrix} 0 & 0 & 0 & 0 & 0 & 0 \\ 0 & H_4^* & H_6^* & BH_3^* & 0 & 0 \\ 0 & P_6^* & P_4^* & BP_3^* & 0 & 0 \\ 0 & BA_4^* & BA_6^* & B^2 A_3^* & 0 & 0 \\ 0 & 0 & 0 & 0 & 0 & 0 \\ 0 & 0 & 0 & 0 & 0 & 0 \end{bmatrix}$$

$$\mathbf{C}_{ae1}^{e} = -\frac{1}{2}\rho U B L_e K \begin{bmatrix} 0 & 0 & 0 & 0 & 0 & 0 \\ 0 & H_1^* & H_5^* & BH_2^* & 0 & 0 \\ 0 & P_5^* & P_1^* & BP_2^* & 0 & 0 \\ 0 & BA_1^* & BA_5^* & B^2 A_2^* & 0 & 0 \\ 0 & 0 & 0 & 0 & 0 & 0 \\ 0 & 0 & 0 & 0 & 0 & 0 \end{bmatrix}$$

The buffeting forces acting on one node of a discrete element of length L_e can be expressed as

$$L_b = \frac{1}{4}\rho U^2 B L_e \left(2C_L \chi_{Lu} \frac{u(t)}{U} + (C_L' + C_D)\chi_{Lw} \frac{w(t)}{U} \right) \tag{13a}$$

$$D_b = \frac{1}{4}\rho U^2 B L_e \left(2C_D \chi_{Du} \frac{u(t)}{U} + C_D'\chi_{Dw} \frac{w(t)}{U} \right) \tag{13b}$$

$$M_b = \frac{1}{4}\rho U^2 B^2 L_e \left(2C_M \chi_{Mu} \frac{u(t)}{U} + C_M'\chi_{Mw} \frac{w(t)}{U} \right) \tag{13c}$$

where L_b, D_b, M_b=lift, drag, and pitching moment force component of buffeting force, respectively; $u(t)$, $w(t)$= longitudinal and vertical turbulent wind fluctuations at the center of the element, respectively; C_L', C_D' and C_D' = partial differentiation of C_L, C_D and C_M with respect to wind attack angle, respectively; $\chi_{Lu}, \chi_{Lw}, \chi_{Du}, \chi_{Dw}, \chi_{Mu}, \chi_{Mw}$= aerodynamic transfer functions between fluctuating oncoming wind velocities and buffeting force, and the absolute magnitude of the functions are so-called aerodynamic admittance.

The multidimensional multivariate velocity fluctuation time histories of turbulent wind with prescribed power spectra can be generated using the weighted amplitude wave superposition method (WAWS) (Deodatis 1996, Shinozuka and Jan 1972). In order to consider the frequency dependent admittance functions, the time histories of wind fluctuations have been generated based on the equivalent power spectrum of turbulent wind fluctuations, which are the product of admittance functions and the wind fluctuating spectrum.

Assuming that the spatial correlations of buffeting forces are the same as those of wind

fluctuations, and wind fluctuation components *u* and *w* are mutually independent, the equivalent power spectrum matrix of turbulent wind fluctuations can be defined as

$$
\mathbf{S} = \begin{bmatrix}
\mathbf{S}_{p_1 p_1} & \mathbf{S}_{p_1 p_2} & \cdots & \mathbf{S}_{p_1 p_n} \\
\mathbf{S}_{p_2 p_1} & \mathbf{S}_{p_2 p_2} & \cdots & \mathbf{S}_{p_2 p_n} \\
\vdots & \vdots & \ddots & \vdots \\
\mathbf{S}_{p_n p_1} & \mathbf{S}_{p_n p_2} & \cdots & \mathbf{S}_{p_n p_n}
\end{bmatrix}
\tag{14}
$$

Where

$$
\mathbf{S}_{p_i p_j} = \begin{bmatrix}
S_{p_i p_j}^{L_k L_k} & S_{p_i p_j}^{L_k D_k} & S_{p_i p_j}^{L_k M_k} \\
S_{p_i p_j}^{D_k L_k} & S_{p_i p_j}^{D_k D_k} & S_{p_i p_j}^{D_k M_k} \\
S_{p_i p_j}^{M_k L_k} & S_{p_i p_j}^{M_k D_k} & S_{p_i p_j}^{M_k M_k}
\end{bmatrix}
\quad , \qquad
S_{p_i p_j}^{L_k L_k} = S_k \left| \chi_{Lk} \right|^2 R_{p_i p_j}
\qquad , \qquad
S_{p_i p_j}^{D_k D_k} = S_k \left| \chi_{Dk} \right|^2 R_{p_i p_j}
\qquad ,
$$

$$
S_{p_i p_j}^{M_k M_k} = S_k \left| \chi_{Mk} \right|^2 R_{p_i p_j} ,
$$

$$
S_{p_i p_j}^{L_k D_k} = S_{p_i p_j}^{D_k L_k} = S_k \sqrt{\left| \chi_{Lk} \right|^2 \left| \chi_{Dk} \right|^2} R_{p_i p_j} , \quad
S_{p_i p_j}^{L_k M_k} = S_{p_i p_j}^{M_k L_k} = S_k \sqrt{\left| \chi_{Lk} \right|^2 \left| \chi_{Mk} \right|^2} R_{p_i p_j} , \quad
R_{p_i p_j} = \exp(-\lambda \frac{\omega r}{2\pi U})
$$

S_k=power spectrum of wind fluctuation component *k* (*k= u, w*); $R_{pi\ pj}$= spatial coherence function of wind fluctuation between points p_i and p_j; λ_j=decay factor, and r_j= distance between p_i and p_j.

Applying WAWS and the equivalent power spectrum of turbulent wind fluctuations, the time history of turbulent wind fluctuation components, modified by aerodynamic admittance, can be obtained.

5. Case Studies

5.1 Jiangdong suspension bridge

Jiangdong Bridge is a three-span suspension bridge with a main span of 260 m and two identical end spans of 83 m each. The heights of its two bridge towers are 97.765 m and 99.915 m. The prestressed concrete bridge deck has a twin-box cross section 47 m wide by 3.5 m high and a central slotting width of 6 m. The bridge deck is supported by inclined hangers at intervals of 9 m. According to observation data, the basic wind speed at the bridge site, namely the yearly-maximum 10-min averaged mean wind speed at 10m height corresponding to a 100-year return period, is 30.6 m/s. According to literature (Xiang 2004), the exponent (α) of mean wind profile at the bridge site is 0.16, and the longitudinal turbulent intensity at deck level is 15%. Thus, the design reference wind speed at deck level (40m above normal water level) for the service state is 38.2 m/s.

The buffeting performance of the bridge is investigated via a full bridge aeroelastic model test at a geometric scale of 1:118 in simulated boundary-layer wind fields with various combinations of wind yaw angle and attack angle in the TJ-3 Boundary Layer Wind Tunnel with a working section

15 m wide, 2 m high and 14 m long. The atmospheric boundary layer is simulated in the TJ-3 wind tunnel using roughness blocks and spirelets, as shown in Fig. 3. The simulated profiles of mean wind and longitudinal turbulent intensities are shown in Figs. 4 and 5, where the gradient height (z_g) is taken as 350 m for terrain type II ($\alpha = 0.16$).
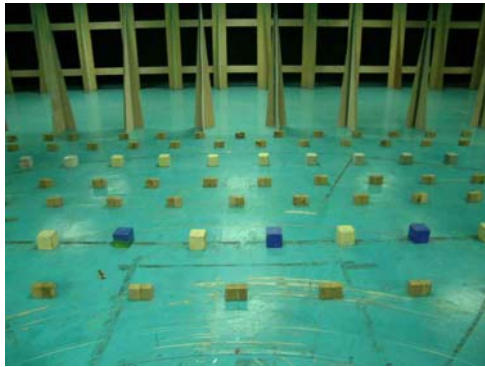

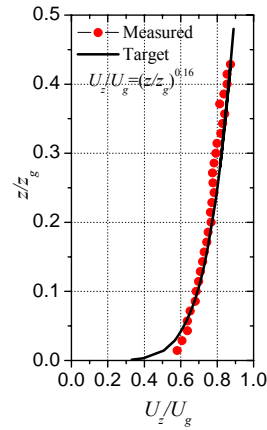Fig. 3 Passive devices for simulation of turbulent wind field of boundary layer
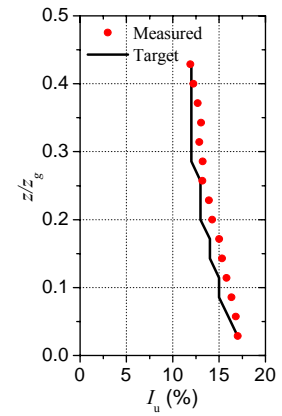
Fig. 4 Profile of mean wind speed

Fig. 5 Profile of longitudinal turbulent intensity

Based on the aerostatic and aerodynamic parameters acquired from a sectional model test as shown in Table 1, numerical buffeting analysis has also been conducted to evaluate the internal buffeting force of the bridge components under normal wind.

Table 1 Parameters used in FEM buffeting analysis of Jiangdong suspension bridge

Aerostatic coefficients						Aerodynamic derivatives			
Lift		Drag		Pitching moment		Lift		Pitching moment	
C_L	C_L'	C_D	C_D'	C_M	C_M'	H_1^*	H_4^*	A_2^*	A_3^*
-0.08	1.45	0.07	-0.04	0.01	0.60	-0.57	-0.11	-0.01	0.01
8	7	72	94	3	1	1	6	8	7

For simulating the numerical equivalent wind field, the spectrum of longitudinal turbulence component $u(t)$ and the vertical turbulence component $w(t)$ are chosen as Simiu and Panofsky functions (Xiang 2004), respectively; the spatial correlation coefficient (λ) is defined as 7.0; and the aerodynamic admittance is defined as the Sears function and 1.0. A time series of simulated equivalent wind fluctuations at the center of the bridge deck at the design wind speed of 38.2 m/s are given in Fig. 6.

In the finite element modeling, the bridge deck, bridge tower and spandrel column are modeled by a 3D-beam element and the main cable and hangers are modeled by a 3D-truss element. The time-averaged aerostatic force, time-varying buffeting force and self-excited force are applied to the bridge components as described above. The corresponding buffeting responses are calculated and compared with the wind tunnel testing results. Fig. 7 shows the wind tunnel tests and the numerical simulation results for the vertical RMS displacements of the bridge deck for 0 attack angle and 0 yaw angle. It is discovered that the numerical results coincide with the wind tunnel test results when the aerodynamic admittance equals the Sears function.
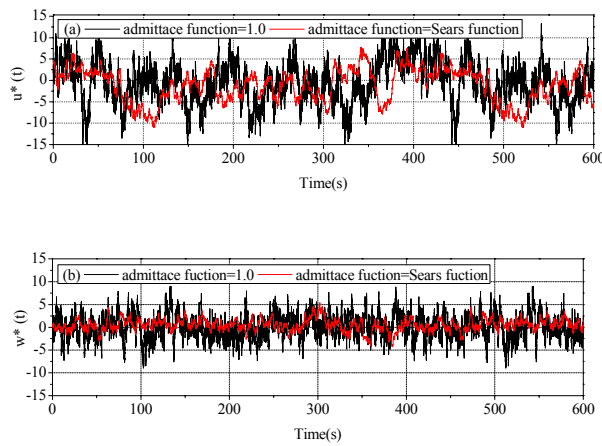
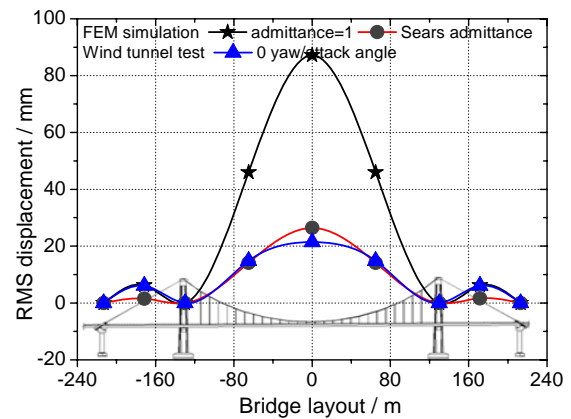Fig. 6 Time series of wind fluctuations (U=38.2 m/s): (a) longitudinal component and (b) vertical component

Fig. 7 Wind tunnel and numerical results for displacements of bridge deck at different span-wise locations

5.1.1 Selection of regressands

The internal structural forces in a linearly elastic structure are decided only by its deformation. The deformation of a structure may be described more precisely with more elements or higher-order elements in finite element analysis, so the computational results may be more precise. In the same way, the significance level of the regressive model may be improved with an increasing number of regressands. However, if the number of regressands is increased, it is necessary to set more sensors to monitor the displacement of different positions on the aero-elastic model in the wind tunnel test. Consequently, it is necessary to choose the minimum number of characteristic displacements without reducing the significance of the regressive model.

The displacements used in the regressive model can be chosen according to the objective internal force, namely the regressor, and the dominant modes that participate in the buffeting response. If there is only one mode participating in the buffeting response and the dominant mode can be fitted with linear functions to a high degree, the internal buffeting force can be fitted with one characteristic displacement to a high confidence level. However, if the only dominant mode in the buffeting response cannot be fitted with linear functions, or the participant modes in buffeting

response are multiple, it is necessary to choose more than one characteristic displacement in the regressive model to make sure the regressive model is of high significance.

Vertical bending mode(0.554Hz)

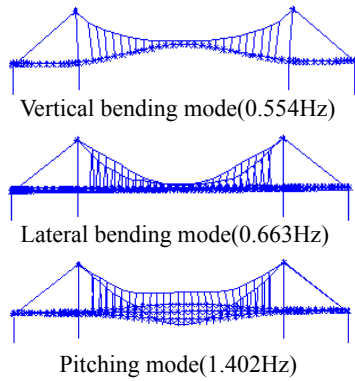Lateral bending mode(0.663Hz)

Pitching mode(1.402Hz)
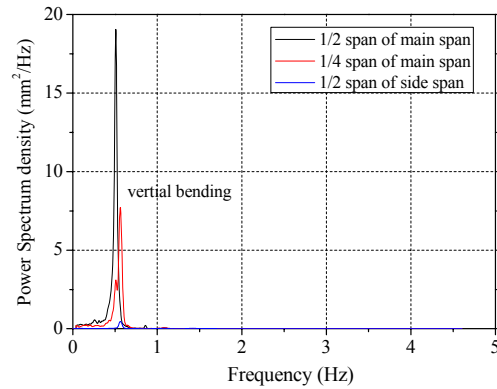
Fig. 8 Fundamental mode of Jiangdong bridge

Fig. 9 PSD of vertical displacement at different spanwise point of bridge deck

The peak energy band of the power spectrum density of turbulent wind concentrates in the low-frequency band. Consequently, the participating modes in buffeting response are mainly some lower order modes. The fundamental vertical, lateral and pitching modes of the bridge deck of Jiangdong Bridge are presented in Fig. 8. In this case study, the objective forces are chosen as the axial forces in the hangers, which are mainly determined by the vertical displacements of the bridge deck and main cable. The power spectrum density of vertical displacements at different spanwise points show that the dominant mode participating in the buffeting response is only the fundamental vertical bending mode, which can be approximately fitted to a linear function, as shown in Fig. 9. Therefore, the vertical buffeting displacement at the center span can be chosen as the regresand.

The regression analysis is conducted based on the time history of buffeting response obtained from numerical analysis. It can be seen that the correlation coefficients between the axial forces in the hangers and the vertical displacements of the center span are all larger than 0.9, as shown in Fig. 10, which indicates that the axial forces in the hangers and the vertical displacements of the center span are linearly correlated to a high confidence level.

5.1.2 Establishment of regressive model

Setting the axial force in the 13th hanger (F_{13}) divided by the horizontal force in the main cable (H), and the buffeting vertical displacement at the center span of bridge deck $v_{t_i} 1/2$ at time t_i, divided by the length of the main span L, the dimensionless regression equation can be expressed as

$$\begin{bmatrix} F_{13}^{t_1}/H \\ \vdots \\ F_{13}^{t_n}/H \end{bmatrix} = \begin{bmatrix} 1 & v_{1/2}^{t_1}/L \\ \vdots & \vdots \\ 1 & v_{1/2}^{t_n}/L \end{bmatrix} \begin{bmatrix} \beta_0 \\ \beta_1 \end{bmatrix}$$
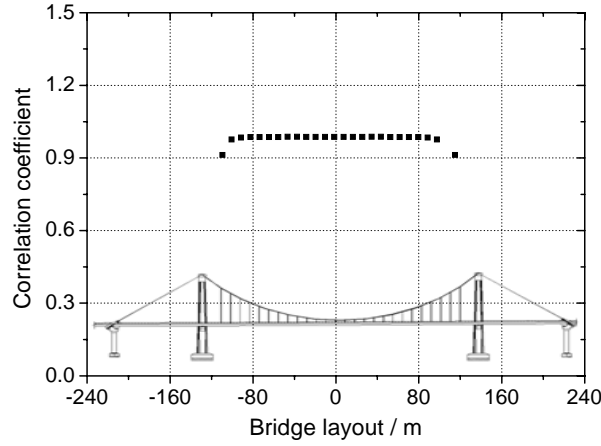
(15)

Fig. 10 Correlation coefficient of mid-span vertical displacement and hanger axial force

Based on the time histories of the buffeting axial force of the 13th hanger and the displacement at the center span acquired from numerical analysis, using the least square method, the coefficients β_i in Eq. (15) can be obtained.

$$\begin{bmatrix} \beta_0 \\ \beta_1 \end{bmatrix} = \begin{bmatrix} 0.06597 \\ 0.01126 \end{bmatrix}$$

(16)

5.1.3 Prediction of internal buffeting force under yaw wind

The buffeting displacements in the regressive model for normal wind are selected according to the dominant modes participating in the buffeting response and the objective internal force. If the dominant modes participating in buffeting response under skew wind with different yaw angles are similar to those for normal wind, and the modal participation ratios, defined in Eq. (17), are almost the same, the regressive model for normal wind can be applied for skew wind.

$$r = \frac{\int_{f_m - \Delta f_m}^{f_m + \Delta f_m} S_\Delta(f) df}{\int_0^{f_t} S_\Delta(f) df}$$

(17)

where r=modal participation ratio; $S_\Delta(f)$= power spectrum density of buffeting displacement obtained in wind tunnel test; f_t= upper limit of model frequency simulated in the full bridge aeroelastic model test; f_m = frequency of specific mode corresponding to the modal participation ratio; Δf_m = maximum allowable deviation of f_m in wind tunnel test.

Table 2 shows that the fundamental vertical bending mode contributes about 90% to the vertical buffeting displacement for both normal wind and skew wind with different yaw angles. Therefore, for engineering application, the error in adopting the regression equation under normal wind to predict the internal forces in bridge components under skew wind case is acceptable.

Table 2 Modal participation ratio of fundamental vertical bending mode

Displacement at different span wise point	Modal participation ratio (%)		
	0deg	22.5deg	45deg
1/2 of middle span	92.7	89.7	91.0
1/4 of middle span	90.4	90.4	92.7

Using the regression equation for normal wind and the buffeting displacement for skew wind obtained from wind tunnel tests, the axial force in the 13th hanger can be easily deduced. The mean and RMS axial stresses in the 13th hanger for skew wind are shown in Table 3. As shown, the buffeting RMS axial stress in the 13th hanger for yaw wind for a 22.5deg yaw angle is larger than that under normal wind.

Table 3 Mean and RMS stress of 13th hanger under skew wind

Yaw angle (deg)	Mean Stress (10^8Pa)	RMS Stress (Pa)
0	3.70705	4160.3
22.5	3.70705	4256.9
45	3.70704	3032.2

5.2 Zhaoqing arch bridge

This steel arch bridge in Guangdong province of China is a half-through arch bridge with a main span of 450 m. Its two inclined arch ribs are 112.5 m from the bottom to the crown and have cross sections of a modified rectangular steel box 5.1 m wide, and 9 m to 15 m from rib base to crown (Fig. 11). The steel-concrete composite girder provides two railway lines supported on arch ribs and columns. According to the literature (Xiang 2004), the basic wind speed at the bridge site is 33.38 m/s and the design reference wind speed at deck level (50.1 m above normal water level) for the service state is 43.2 m/s; the exponent (α) of mean wind profile at the bridge site is 0.16; and the longitudinal and vertical turbulent intensities at deck level are 15% and 13.2%, respectively.

A full bridge aero-elastic model test at a geometric scale of 1:70 is also carried out in the TJ-3 Wind Tunnel in Tongji University to investigate the buffeting performances of the bridge under yaw winds. The simulated profiles of mean wind and longitudinal and vertical turbulent intensities are shown in Figs. 12-14.
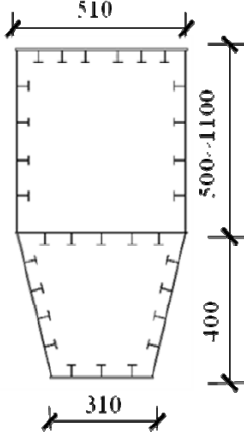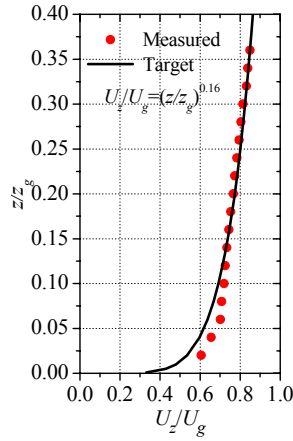
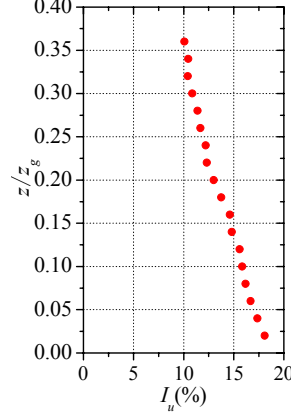Fig. 11 Cross section of arch ribs

Fig. 12 Profile of mean wind speed

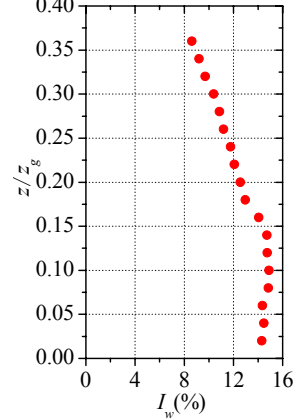Fig. 13 Profile of longitudinal turbulent intensity

Fig. 14 Profile of vertical turbulent intensity

Zhao and Ge (2009) pointed out that the FE buffeting analysis results may be incorrect if the Sears function or 1.0 are applied as admittance functions, and the section of the arch ribs is so bluff that it is necessary to identify the aerodynamic admittance function of the modified rectangular section to improve the precision of buffeting analysis. In the present paper, equivalent aerodynamic admittance functions for this bluff box section are defined and used in the numerical analysis.

$$\left|\chi'_{Lu}\right|^2 = \left|\chi'_{Lw}\right|^2 = \frac{4C_L^2\left|\chi_{Lu}\right|^2 S_u(\omega) + \left(C'_L + C_D\right)^2\left|\chi_{Lw}\right|^2 S_w(\omega)}{4C_L^2(\alpha) S_u(\omega) + \left(C'_L + C_D\right)^2 S_w(\omega)} \tag{18}$$

$$\left|\chi'_{Du}\right|^2 = \left|\chi'_{Dw}\right|^2 = \frac{4C_D^2\left|\chi_{Du}\right|^2 S_u(\omega) + C_D'^2\left|\chi_{Dw}\right|^2 S_w(\omega)}{4C_D^2(\alpha) S_u(\omega) + C_D'^2 S_w(\omega)} \tag{19}$$

$$\left|\chi'_{Mu}\right|^2 = \left|\chi'_{Mw}\right|^2 = \frac{4C_M^2\left|\chi_{Mu}\right|^2 S_u(\omega) + C_M'^2\left|\chi_{Mw}\right|^2 S_w(\omega)}{4C_M^2(\alpha) S_u(\omega) + C_M'^2 S_w(\omega)} \tag{20}$$

where $|\chi'_{Lu}|^2$, $|\chi'_{Lw}|^2$, $|\chi'_{Du}|^2$, $|\chi'_{Dw}|^2$, $|\chi'_{Mu}|^2$, $|\chi'_{Mw}|^2$ = equivalent aerodynamic admittance.

The measured equivalent aerodynamic admittance functions of the modified rectangular section in turbulent wind with 11% turbulence intensity are shown in Fig. 15.

For finite element modeling, the bridge deck, arch ribs, arch bracing and spandrel column are modeled by a 3D-beam element and the hangers are modeled by a 3D-truss element. For simulation of a numerical equivalent wind field, the spectrum of longitudinal turbulence component $u(t)$ and the vertical turbulence component $w(t)$ are chosen as Simiu and Panofsky functions (Xiang 2004), respectively, and the spatial correlation coefficient is defined as 7.0. The aerodynamic and structural parameters used in the FE buffeting analysis under normal wind are

presented in Table 4.
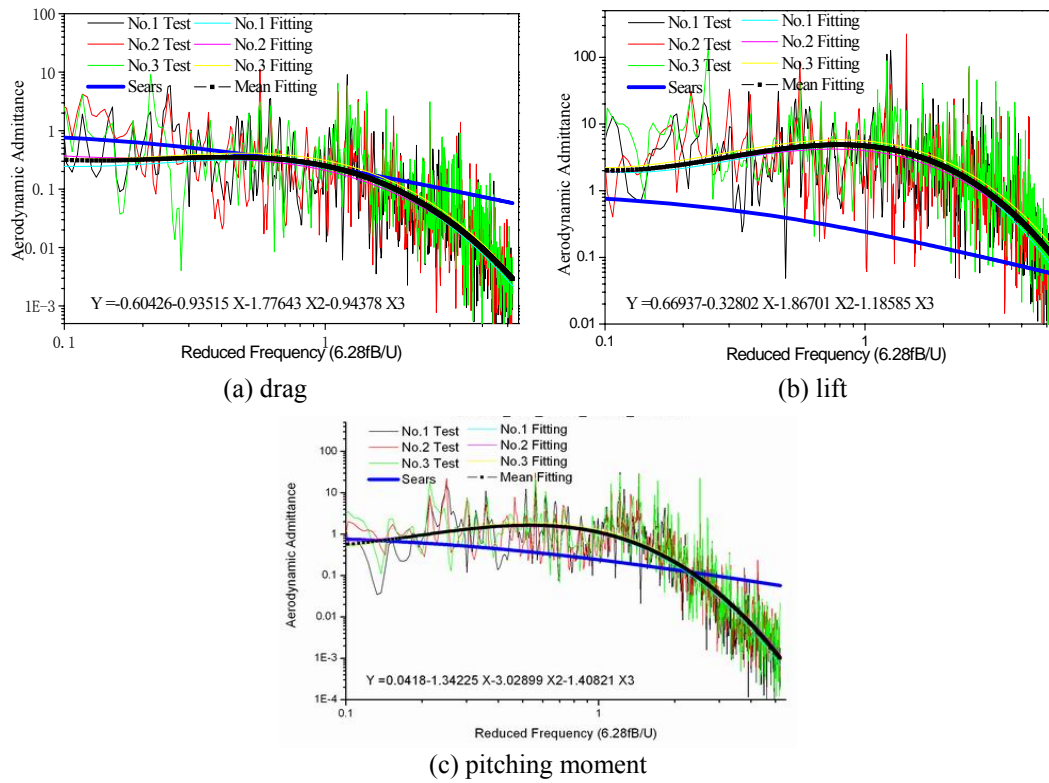

(a) drag

(b) lift

(c) pitching moment

Fig. 15 Aerodynamic admittance function of modified rectangular section of arch ribs

Table 4 Parameters used in stochastic FEM buffeting analysis of Zhaoqing arch bridge

Structural components	Aerostatic coefficients						Aerodynamic derivatives			
	Lift		Drag		Pitching moment		Lift		Pitching moment	
	C_L	C_L'	C_D	C_D'	C_M	C_M'	H_1^*	H_4^*	A_2^*	A_3^*
Arch ribs	0.055	0.057	0.67	-0.088	0.136	-0.017	0.9312	0.1202	-0.0783	0.0738
Bridge deck	-0.062	0.098	0.183	-0.066	-0.006	0.0175	-0.305	0.467	-0.0257	-0.0319

The corresponding buffeting responses are calculated and compared to the wind tunnel testing results. Fig. 16 shows that the numerical results are in very good agreement with the wind tunnel test results, which indicates that the numerical model and parameters used in the numerical simulation are reasonable and reliable.

5.2.1 Selection of regressands

In this case, the objective regression forces are the six internal force components at the center span of the arch ribs. The power spectrum density of lateral and vertical buffeting displacement of

the 1/2, 3/8, 1/4, and 1/8 spanwise points of the arch ribs indicate that the dominant modes participating in buffeting displacement are the first lateral bending mode and the first symmetric and asymmetric vertical modes, as shown in Fig. 17.
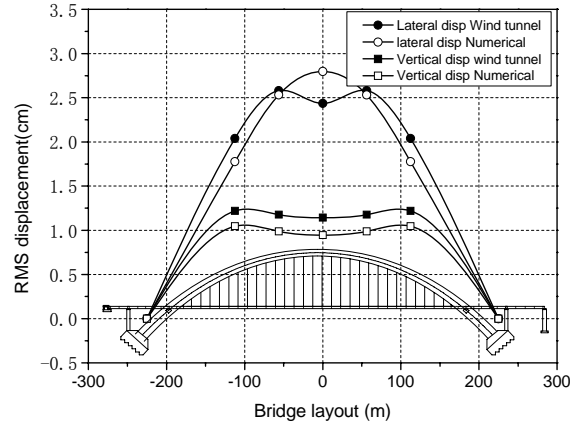

Fig. 16 Numerical analysis and wind tunnel test results of arch ribs

(a) PSD of arch ribs lateral displacement   (b) PSD of arch ribs vertical displacement
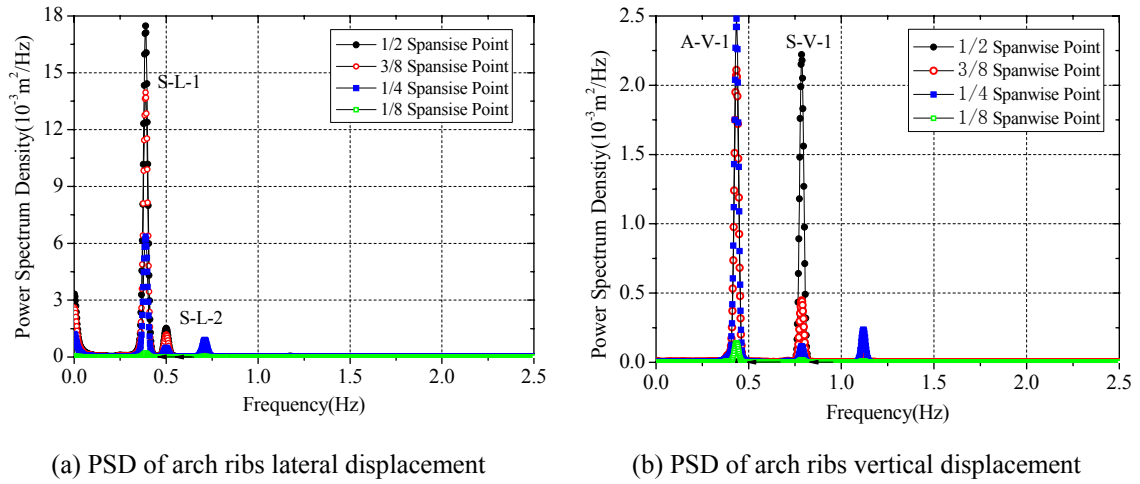
Fig. 17 PSD of arch ribs displacement at different spanwise points

The first and second vertical and lateral modes are presented in Table 5. Obviously, the first two vertical and lateral bending mode shapes cannot be fitted with linear functions. Consequently, in the regressive model, it is necessary to include $v_{1/2}$, $v_{3/8}$, $v_{1/4}$, $h_{1/2}$, $h_{3/8}$, $h_{1/4}$, namely the vertical and lateral displacements of the 1/2, 3/8, 1/4 of arch ribs, which are characteristic points of the first

two vertical and lateral modes.

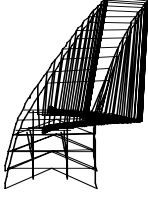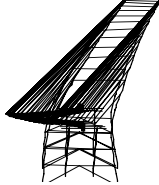Table 5 First and second vertical and lateral modes of numerical example

1st symmetric lateral bending (S-L-1) 0.3843Hz	1st asymmetric vertical bending (A-V-1) 0.4381Hz	2nd symmetric lateral bending (S-L-2) 0.4898Hz	1st symmetric vertical bending (S-V-1) 0.7810Hz

Fig. 18 shows the correlation coefficients between the internal forces at the center of the arch ribs and the displacements at different span-wise points of the arch ribs. When the regressive displacements are less than $v_{1/2}$, $v_{3/8}$, $v_{1/4}$, $h_{1/2}$, $h_{3/8}$, $h_{1/4}$, the coefficients decrease sharply. Some are less than 0.8, which indicates that the linear relation is not significant. However, when the regressive displacements are more than $v_{1/2}$, $v_{3/8}$, $v_{1/4}$, $h_{1/2}$, $h_{3/8}$, $h_{1/4}$, the correlation coefficients do not obviously increase. Therefore, $v_{1/2}$, $v_{3/8}$, $v_{1/4}$, $h_{1/2}$, $h_{3/8}$, $h_{1/4}$ may be a proper regressand group.
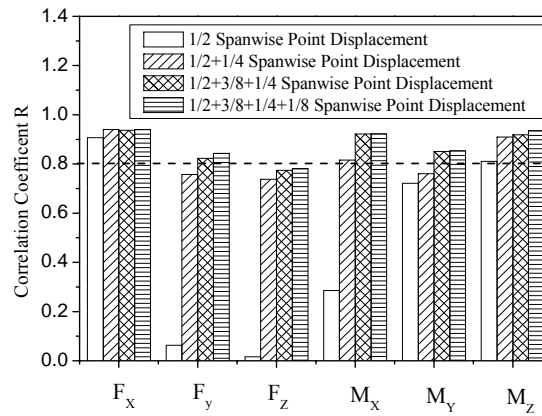

Fig. 18 Correlation coefficients vs. the regressands

5.2.2 Establishment of regressive model

With the vertical and lateral displacements at the 1/2, 3/8, and 1/4 span-wise points of the arch ribs as the regressive displacements, the internal forces at the center of the arch ribs as objective regression forces, determined from Eq. (1), the regression equations are

$$F_i = \overline{\beta}_{0i} + \overline{\beta}_{1i}v_{1/2} + \overline{\beta}_{2i}h_{1/2} + \overline{\beta}_{3i}v_{3/8} + \overline{\beta}_{4i}h_{3/8} + \overline{\beta}_{5i}v_{1/4} + \overline{\beta}_{6i}h_{1/4} \left(i = 1,2,\cdots 6\right) \qquad (21)$$

where $F_i=j$th internal force component at the center of the arch ribs; setting F_i divided by F_{gi},

namely the *i*th internal force component at the center of the arch ribs induced by gravity, and $v_{1/2}$, $v_{3/8}$, $v_{1/4}$, $h_{1/2}$, $h_{3/8}$, $h_{1/4}$ divided by H, namely the height of the arch ribs at the mid-span section, Eq. (21) can be converted to dimensionless, as

$$\mathbf{F} = \mathbf{\Delta}\mathbf{\beta} \tag{22}$$

where $\mathbf{F} = \begin{bmatrix} F_1^{t_1} & \cdots & F_6^{t_1} \\ \vdots & \vdots & \vdots \\ F_1^{t_n} & \cdots & F_6^{t_n} \end{bmatrix} \begin{bmatrix} F_{g1} & \cdots & 0 \\ \vdots & \vdots & \vdots \\ 0 & \cdots & F_{g6} \end{bmatrix}^{-1}$, $\mathbf{\Delta} = \dfrac{1}{H} \begin{bmatrix} H & v_{1/2}^{t_1} & h_{1/2}^{t_1} & v_{3/8}^{t_1} & h_{3/8}^{t_1} & v_{1/4}^{t_1} & h_{1/4}^{t_1} \\ \vdots & \vdots & \vdots & \vdots & \vdots & \vdots & \vdots \\ H & v_{1/2}^{t_n} & h_{1/2}^{t_n} & v_{3/8}^{t_n} & h_{3/8}^{t_n} & v_{1/4}^{t_n} & h_{1/4}^{t_n} \end{bmatrix}$,

$\mathbf{\beta} = \begin{bmatrix} \beta_{01} & \cdots & \beta_{06} \\ \vdots & \vdots & \vdots \\ \beta_{61} & \cdots & \beta_{66} \end{bmatrix}$

The internal forces at the center of the arch ribs induced by gravity are presented in Table 6.

Table 6 Mid-span internal force of arch ribs induced by gravity

F_{g1} (N)	F_{g2}(N)	F_{g3}(N)	F_{g4}(Nm)	F_{g5}(Nm)	F_{g6}(Nm)
-7.36E+06	-7.87E+06	6.08E+05	-9.63E+05	-6.63E+05	-1.32E+07

Based on the time history of the internal forces and displacements of the arch ribs obtained from the numerical analysis, the coefficients $\mathbf{\beta}$ in Eq. (22) can be obtained using the least square method. Subsequently, significance testing of the regressive model and regression coefficients is conducted for 99% confidence level and the results are presented in Table 7. Obviously, the statistical variable $\tilde{F}$ of the internal forces at the center of the arch ribs are all larger than $\tilde{F}_\alpha$, namely the critical value of the F-test in 99% confidence level. Therefore, the null hypothesis of the regressive model should be rejected and the linear correlation of the regressive model should be considered to be significant. As well, the statistical indictors $|t_i|(i=1,2,\ldots6)$ of F_1/F_{g1}, F_3/F_{g3}, F_4/F_{g4}, F_5/F_{g5}, F_6/F_{g6} are larger than t_α, namely the critical value of the t-test in 99% confidence level, so the null hypothesis can be rejected and the linear correlation relations between F_1/F_{g1}, F_3/F_{g3}, F_4/F_{g4}, F_5/F_{g5}, F_6/F_{g6} and $v_{1/2}/H$, $v_{3/8}/H$, $v_{1/4}/H$, $h_{1/2}/H$, $h_{3/8}/H$, $h_{1/4}/H$ are significant. However, the statistical indictor $|t_6|$ of F_2/F_{g2} is smaller than t_α, so the linear correlation relation between F_2/F_{g2} and $h_{1/4}/H$ is not significant. The exclusion of $h_{1/4}/H$ from the regression calculation of F_2/F_{g2} may not decrease the significance of the regressive model.

The regressive model between internal buffeting force at the center of the arch ribs and the displacements at 1/2, 3/8 and 1/4 span-wise point of the arch ribs is

$$\mathbf{F} = \mathbf{\Delta} \begin{bmatrix} -9.62 & -1.95 & -4.28 & 0.56 & 4.96 & -14.5 \\ 58.82 & -204.17 & -115.27 & -51.31 & 150 & -369.11 \\ 13.46 & 11.89 & -684.63 & 796.57 & -1032.6 & 4.98 \\ -14.57 & 354 & 154.67 & 115.29 & -206.18 & 168.89 \\ 27.94 & -12.35 & 932.45 & -1362.83 & 2444.54 & -11.54 \\ 13.94 & 242.58 & -147.2 & -106.51 & 192.8 & -100.69 \\ -33.9 & 0.0 & -236.47 & 632.95 & -1569.8 & 6.61 \end{bmatrix} \qquad (23)$$

Table 7 Significance testing of regressive model and regression coefficients

	$\tilde{F}$	$\tilde{F}_\alpha$	R	$|t_1|$	$|t_2|$	$|t_3|$	$|t_4|$	$|t_5|$	$|t_6|$	t_α
F_1/F_{g1}	2986	2.8	0.9369	400	107	112	244	168	434	2.3
F_2/G_{g2}	869	2.8	0.8225	432	32	848	35	908	*0.89*	2.3
F_3/F_{g3}	622	2.8	0.7743	43	298	65	454	97	166	2.3
F_4/F_{g4}	2341	2.8	0.9216	39	708	99	1353	143	906	2.3
F_5/F_{g5}	1094	2.8	0.8513	42	338	65	894	96	828	2.3
F_6/F_{g6}	2245	2.8	0.9186	938	15	487	38	453	32	2.3

By substituting the numerical buffeting displacements at 1/2, 3/8 and 1/4 span-wise points of the arch ribs in Eq. (23), the six internal force components at the center of the arch ribs can be obtained. Fig. 19 compares the regression and numerical analysis results for six internal force components at the center of the arch ribs. The regression results show very good agreement with those from the numerical analysis.

5.2.3 Prediction of internal buffeting force under skew wind

The modal participation coefficients of the first lateral bending mode, the first symmetric and asymmetric mode in the buffeting displacements under normal wind and skew wind case, are shown in Table 8. The contribution ratios of the first lateral bending mode, and the sum of the first symmetric and asymmetric mode in the buffeting displacement, all exceed 90%, which indicates that the dominant modes participating in the buffeting response are similar for normal wind and skew wind. The similarity of the dominant modes and their corresponding participation ratio verify that the regressive model deduced under normal wind can be applied to predict the internal force of bridge components under skew wind.

The time history of buffeting internal force components at the center of arch ribs can be obtained by applying the regressive model and the time history of buffeting displacements at different span points of the arch ribs under yaw wind for different yaw angles from the full bridge aero-elastic wind tunnel test. The numerical RMS displacements at different span points of the arch ribs fit well with those from the wind tunnel test under normal wind, and the regressive model under normal wind can be applied to skew wind. Thus, the RMS of internal buffeting force based on the regressive model under normal wind and the time history of the buffeting displacements from the aero-elastic model wind tunnel test can be considered to be reliable.
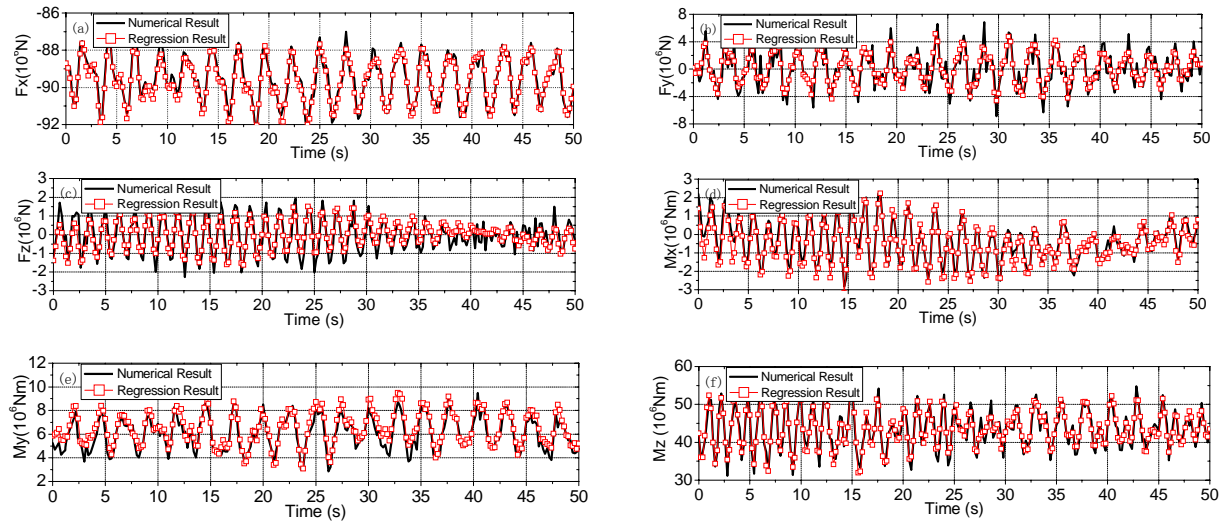
Fig. 19 Comparison of the internal force components at center of arch ribs: (a) F_x, (b) F_y, (c) F_z, (d) M_x, (e) M_y and (f) M_z

Table 8 Modal participation ratio of dominant modes

Displacement at different span wise points	Mode	Modal participation ratio (%)			
		0deg	15deg	30deg	45deg
1/2	S-L-1	94.3	96.1	92.8	91.7
	A-V-1	13.0	30.0	22.1	28.7
	S-V-1	60.4	62.4	62.4	40.8
1/4	S-L-1	93.6	93.0	80.0	89.1
	A-V-1	91.5	93.4	94.0	94.2
	S-V-1	3.5	2.1	1.9	1.1
3/8	S-L-1	95.8	98.9	92.6	94.4
	A-V-1	94.5	94.0	95.1	95.5
	S-V-1	1.1	2.6	0.3	0.2

Fig. 20 shows the RMS and extreme values of internal forces at the center of the arch ribs, assuming a peak factor of 4.0. As shown in Fig. 20, the RMS and extreme values of internal forces at the center of the arch ribs for the yaw wind case for 15deg and 30deg yaw angle are larger than those under normal wind.
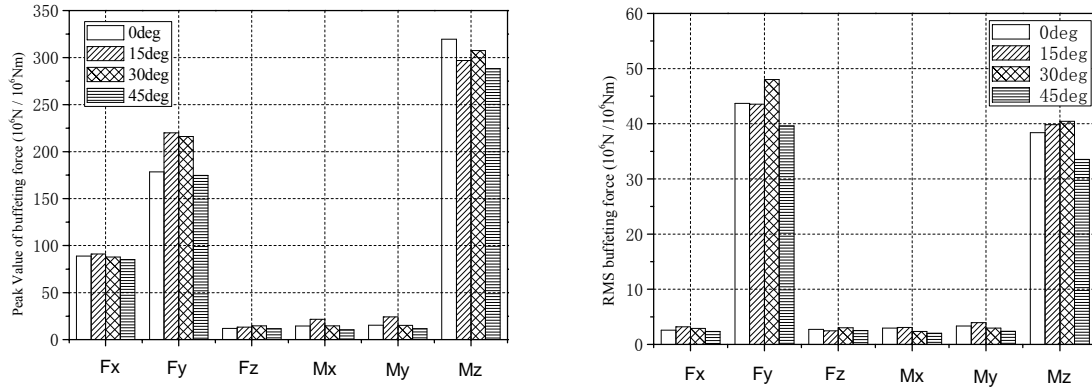
(a) Extreme value of internal buffeting force components   (b) RMS internal buffeting force components

Fig. 20 Prediction of mid-span internal buffeting force components in arch ribs

6. Conclusions

A new analysis framework used to predict the internal forces in bridge components under skew wind is presented in this paper. The regression analysis of the Jiangdong suspension bridge and the Zhaoqing arch bridge demonstrate the accuracy and effectiveness of the proposed framework. This framework combines full bridge aero-elastic wind tunnel testing and numerical buffeting simulation. Before the regression analysis, it is necessary to conduct a numerical analysis to check and modify the finite element model until the numerical results fit well with the wind tunnel test results. The displacements in the regressive model should be selected according to the objective regression forces and the shape of participant dominant modes to improve the significance of the regressive model. The dominant modes that participate in the buffeting response under yaw wind for different yaw angles and their corresponding participation ratios should be similar in order to guarantee that the regressive model for normal wind can be used for yaw wind. The internal buffeting forces in bridge components can be obtained based on the regressive model under normal wind and the time history of buffeting displacement from aero-elastic model wind tunnel tests. The internal buffeting forces of bridge components may reach the extreme value for yaw wind.

7. Acknowledgments

References

Borri, C., Costa, C. and Zahlten, W. (2002), "Non-stationary flow forces for the numerical simulation of aeroelastic instability of bridge decks", *Comput. Struct.*, **80**(12), 1071-1079.

Davenport, A.G. (1962), "Buffeting of a suspension bridge by storm winds", *J. Struct. Division*, **88**(3), 233-268.

Deodatis, G. (1996), "Simulation of ergodic multivariate stochastic processes", *J. Eng. Mech.- ASCE.,* **122**(8), 778-787.

Ge, Y.J. and Tanaka, H. (2000), "Aerodynamic flutter analysis of cable-supported bridges by multi-mode and full-mode approaches", *J. Wind Eng. Ind. Aerod.,* **86**, 123-153.

Kimura, K. and Tanaka, H. (1992), "Bridge buffeting due to wind with yaw angles", *J. Wind Eng. Ind. Aerod.*, **42**(1-3), 1309-1320.

Lin, Y. (1979), "Motion of suspension bridges in turbulent winds", *J. Eng. Mech. - ASCE.*, **105**(6), 921-932.

Lin, Y.K. and Li, Q.C. (1983), "Multimode bridge response to wind excitations", *J. Eng. Mech. - ASCE*, **119**(1), 113-127.

Salvatori, L. and Borri, C. (2007), "Frequency-and time-domain methods for the numerical modeling of full-bridge aeroelasticity", *Comput. Struct.*, **85**(11-14), 675-687.

Scanlan, R. (1978), "The action of flexible bridges under wind, II: Buffeting theory", *J. Sound Vib.*, **60**(2), 201-211.

Scanlan, R.H. (1993a), "Bridge buffeting by skew winds in erection stages", *J. Eng. Mech. - ASCE.*, **119**(2), 251-269.

Scanlan, R.H. (1993b), "Problematics in formulation of wind-force models for bridge decks", *J. Eng. Mech. - ASCE*, **119**(7), 1353-1375.

Scanlan, R.H. (2000), "Bridge deck aeroelastic admittance revisited", *J. Bridge Eng.*, **5**(1), 1-7.

Shinozuka, M. and Jan, C.M. (1972), "Digital simulation of random processes and its applications", *J. Sound Vib.*, **25**(1), 111-128.

Xiang, H.F. (2004), "Wind-resistent design specification for highway bridges", JTG/T D60-01-2004, People's Communication Press (in Chinese).

Xie, J., Tanaka, H., Wardlaw, R. and Savage, M. (1991), "Buffeting analysis of long span bridges to turbulent wind with yaw angle", *J. Wind Eng. Ind. Aerod.*, **37**(1), 65-77.

Zhao, L., Ge, Y. and Zhu, L. (2008), "Wind-excited vibration of long-span steel-lattice arch bridge under typhoon climate", *Proceeding of the 4th International Conference on Advances in Wind and Structures*. Jeju, Korea

Zhu, L., Xu, Y. and Xiang, H. (2002), "Tsing Ma bridge deck under skew winds--Part II: flutter derivatives", *J. Wind Eng. Ind. Aerod.*, **90**(7), 807-837.

Zhu, L., Xu, Y., Zhang, F. and Xiang, H. (2002), "Tsing Ma bridge deck under skew winds--Part I: Aerodynamic coefficients", *J. Wind Eng. Ind. Aerod.*, **90**(7), 781-805.

Zhu, L. and Xu, Y. (2005), "Buffeting response of long-span cable-supported bridges under skew winds. Part 1: theory", *J. Sound Vib.*, **281**(3-5), 647-673.

Zhu, L., Wang, M., Wang, D., Guo, Z. and Cao, F. (2007), "Flutter and buffeting performances of Third Nanjing Bridge over Yangtze River under yaw wind via aeroelastic model test", *J. Wind Eng. Ind. Aerod.*, **95**(9-11), 1579-1606.

CC